Technische Universität München
Fakultät für Physik

Abschlussarbeit im Bachelorstudiengang Physik

Entwicklung und Charakterisierung eines Detektors mit COBRA GEMs

Development and Characterization of a Detector Based on COBRA GEMs

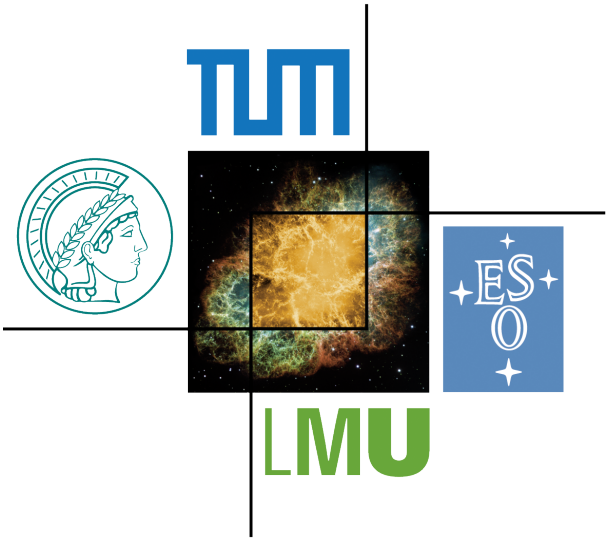

Thomas Klemenz

2. September 2016

Erstgutachter (Themensteller): Prof. L. Fabbietti
Zweitgutachter: Prof. E. Resconi

Contents

Abstract

In modern experimental physics at accelerator facilities detector systems have to fulfil high demands. In TPCs one of these is a high readout rate combined with a low ion back flow due to high event rates in collider experiments. Therefore the gated MWPC which is widely used in TPCs is no longer an option since it limits the detection rate. GEM foils were introduced as a viable alternative providing continuous readout and intrinsic ion back flow suppression. Another type of GEM, the COBRA GEM, was developed to provide an even better suppression of the ion back flow. In this Bachelor's Thesis a COBRA GEM is designed and its energy resolution, effective gain and ion back flow reduction capability are studied.

Chapter 1

Introduction

In today's experimental physics at accelerator facilities, high requirements are put on the particle detector systems. Not only are high precision measurements demanded concerning momentum and spatial resolution but also high detection rates are very important to cope with the amount of events in high luminosity particle collisions. Thus the detectors have to handle high radiation doses and provide a fast readout system. The Time Projection Chamber (TPC) [1], a 3D-tracking system, fits these high demands when combined with Gas Electron Multiplier (GEM) foils [2].

GEMs allow to operate a TPC ungated i.e. continuously, leading to higher detection rates since they replace gated Multi Wire Proportional Chambers (MWPCs) for providing electron multiplication and ion back flow (IBF) reduction. Recently a new device called COBRA GEM [3] was introduced as an alternative to GEM foils to potentially yield better IBF suppression. In this thesis the energy resolution, the effective gain and the IBF reduction capability of a single COBRA GEM were studied.

1.1 Time Projection Chamber

A TPC [1] is a gas filled, often cylindrical volume with electrodes on both ends to apply an electrical field. Due to this drift field electrons and ions created by a traversing ionizing particle drift towards the anode or cathode respectively. These electrons are called primary electrons. Because of their mass, the drift velocity of the electrons is approximately 1000 times higher compared to the ions. At their arrival the electrons induce signals in the segmented anode. Due to this segmentation it is possible to reconstruct the position where the electron reached the anode. Combining this position with the electron drift time one can reconstruct the point of ionization in three dimensions. Thus a full 3D-tracking of ionizing particles can be realised with a TPC. When the TPC is placed inside a magnetic field the particle trajectory describes a helix with a radius proportional to its charge, mass and velocity. Using an external time-of-flight (TOF) measurement to identify the velocity one can calculate the mass of the particle.

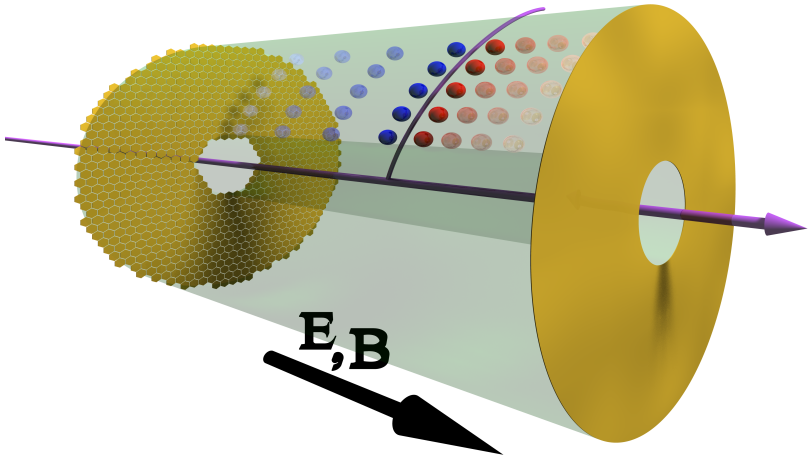

Figure 1.1: Schematic drawing of a TPC, for more details see text [4]

Fig. 1.1 shows a schematic drawing of a TPC. The green area depicts the gas volume. The yellow plate on the left is the segmented anode, the one on the right is the cathode. The beam and particle trajectory are shown in purple. The blue and red dots are the electrons and ions with increasing transparency as a function of time.

Often TPCs have a hole along their center line where beam pipes pass trough the detector. Either a fixed target or the interaction point of two particle beams can be placed in this hole when used in a collider experiment. Particles produced in collisions pass through the gas volume of the TPC and generate electron ion pairs upon impact ionization. Since in average only one to two electron ion pairs are produced in each collision of the traversing particle with a gas molecule, the induced signal at the anode is not high enough to be observed by the readout electronics. Hence the electrons have to be multiplied. In conventional TPCs MWPCs [5] are used for that purpose. MWPCs consist of at least two layers of wires parallel to the anode. The layer closer to the anode is the anode wire grid followed by the cathode wire grid (see fig. 1.2). Potentials are applied to the grids in a way that very high fields are reached at the anode wires in order to create electron avalanches by arriving primary electrons. While the electrons drift towards the anode wires and do not contribute to the signal, the ions created in this process drift towards the cathode wires and create mirror charges in the anode. These mirror charges induce a signal which can be read out. While most of the ions reach the cathode wires a significant amount of ions can infringe on the active area of the TPC and drift towards the cathode. This process is called ion back flow. Those ions distort the drift field by building up space charges.

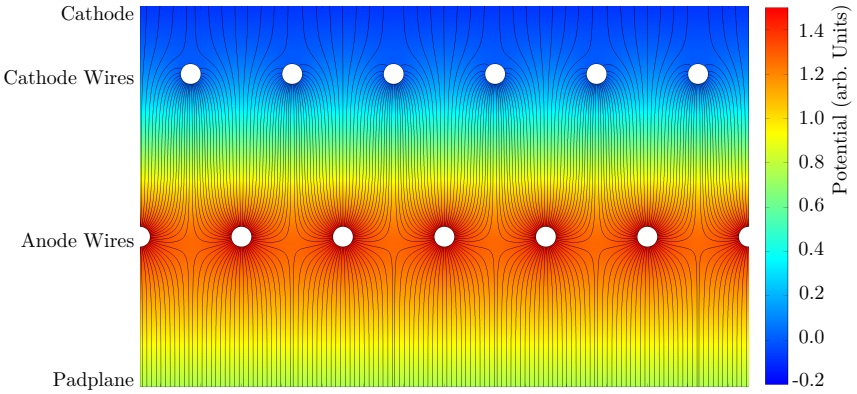

Figure 1.2: Exemplary potential configuration in a MWPC. The field lines are depicted in black, the cross section of the wires is white and the potential is colored [4]

However a homogeneous drift field is mandatory to measure the correct drift time and impact point of electrons at the anode to reconstruct the proper trajectory of particles traversing the TPC. To reduce the amount of ions drifting into the active volume, a third layer of wires, the gating grid, is placed above the cathode wires. This gating grid can be enabled by applying a potential in a way that all field lines end on the wires of the gating grid. This forces the ions produced in the avalanche to drift towards the gating grid where they are neutralised. After all ions have reached the gating grid, it is disabled. When the gating grid is disabled it is transparent for electrons but when it is enabled, no electrons can reach the amplification area hence the detector is blind during this time. Therefore the gating grid limits the detection rate. In case of the ALICE TPC [6] for example the readout rate is limited to 3.5 kHz for proton-proton collisions. However with the high interaction rates after the high luminosity upgrade of the LHC [7] a continuous readout is needed so the gated MWPC is not an option anymore. Using GEM foils instead of MWPCs for electron multiplication makes the use of a gating grid redundant since they provide an intrinsic IBF reduction.

1.2 GEM foils

A GEM foil [2] consists of an insulator foil (thickness: 50 µm) clad with copper on both sides. As insulator material Kapton is often used. By electrochemical etching, the foil is perforated with a regular pattern of double conically shaped holes. The perforated area is called active area. Fig. 1.3 shows the dimensions of a standard

GEM foil. By applying a potential difference of several hundred volts between the two copper layers, an electric field in the order of $1000\,\frac{\mathrm{V}}{\mathrm{cm}}$ can be reached in the holes.

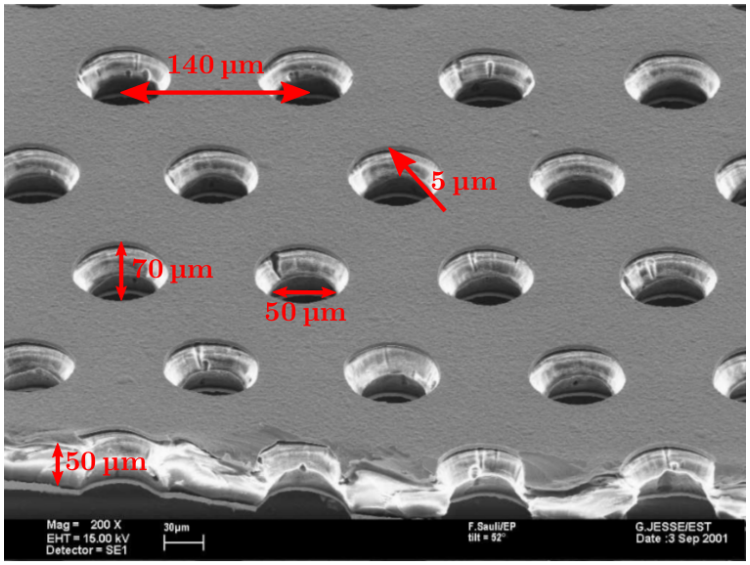

Figure 1.3: Dimensions of a standard GEM foil

When a GEM foil is placed inside the electric field of a TPC instead of a MWPC, a field configuration like in fig. 1.4 ensues. The primary electrons drift towards the upper side of the GEM where they are collected into the holes and avalanche amplification appears due to the high field strength inside the holes. Then the electrons are extracted at the bottom side of the GEM and can be accelerated either towards another GEM foil for further amplification or towards the anode for readout. By using more than one GEM foil an effective gain in the order of $\approx 10^4$ can easily be reached. The gain of a GEM foil is actually higher than the effective gain. The gain is defined as:

$$G = \frac{\text{number of electrons produced in the avalanche amplification}}{\text{number of primary electrons}} \tag{1.1}$$

However the extraction efficiency

$$\alpha = \frac{\text{number of electrons extracted from the GEM holes}}{\text{number of electrons produced in the avalanche amplification}} \tag{1.2}$$

is not 100 %. The effective gain is defined as:

$$G_{\text{eff}} = \frac{I_{\text{A}}}{I_{\text{prim}}} \tag{1.3}$$

with I_{A} being the current at the anode and I_{prim} the primary current which results from the primary electrons. Since the effective gain only takes the electrons extracted from the GEM holes into account, it is lower than the gain.

The big asset of the GEM foil, the intrinsic ion back flow reduction, appears when it is operated in an asymmetric field where the electric field below the GEM is stronger than above the GEM. In this case some of the field lines end on the top side of the GEM (see fig. 1.4), forcing a significant amount of the ions created in the avalanche to drift towards the upper surface of the foil where they are neutralized. Therefore they can not penetrate the drift volume and do not distort the drift field. By stacking GEM foils not only the gain but also the IBF suppression can be improved. With a stack of three GEM foils and an optimized voltage setting as well as optimizations concerning the hole pitch and pattern, an IBF of 0.4 % [8] can be reached. Nevertheless, offline corrections of the data due to the distortions introduced by the remaining ions reaching the drift region have to be applied. However, when online data analysis has to be done to reduce the amount of data which has to be processed, these offline corrections cannot be applied since the remaining IBF adulterates such online analysis. A possibility to render the online analysis feasible are COBRA GEMS as they can provide a better IBF reduction compared to conventional GEM foils.

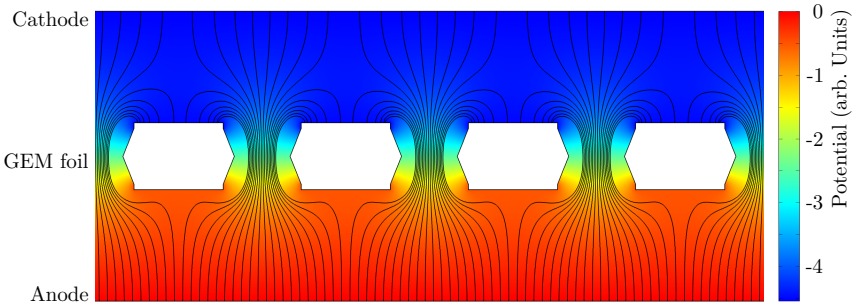

Figure 1.4: Exemplary potential configuration of a GEM foil. The field lines are depicted in black, the cross section of the GEM foil is white and the potential is colored [4]

Chapter 2

Thick COBRA GEM

In this chapter the structure and the design of a thick COBRA GEM are discussed.

2.1 Structure of a thick COBRA GEM

Just like conventional GEMs, thick COBRA GEMs consist of an insulator (usually FR 4 or FR 5) clad with copper on both sides. Due to the thickness of the insulator (400 µm), the COBRA GEMs used in this work rank among the thick GEMs (THGEMs). On either one or both sides the characteristic structure is etched into the copper surface creating two electrodes. In the following these electrodes are called COBRA structure (C) and copper area (A) (see fig. 2.1). The holes of the thick COBRA GEM have to be drilled in contrast to the standard GEM, where the holes can be etched into the insulator. This limits the hole size to 100 µm at minimum. In this experiment a GEM with a COBRA structure only on the top side was used. The dimensions as partly depicted in fig. 2.2 are shown in table 2.1. In this work $\Delta U_{\mathrm{AC}} = U_{\mathrm{A}} - U_{\mathrm{C}}$ with U_{A} being the potential at the copper area and U_{C} at the COBRA structure.

insulator thickness	400 µm
hole diameter	300 µm
hole pitch	1 mm
rim width	100 µm
metal width	100 µm
metal thickness	15 µm
active area	35 mm × 35 mm

Table 2.1: Dimensions of the COBRA GEM used in the experiment

Fig. 2.3 shows the result of a finite element calculation taking the COBRA geometry into account. At $\Delta U_{\mathrm{AC}} = 0\,\mathrm{V}$ the field is similar to a standard GEM foil (see fig.

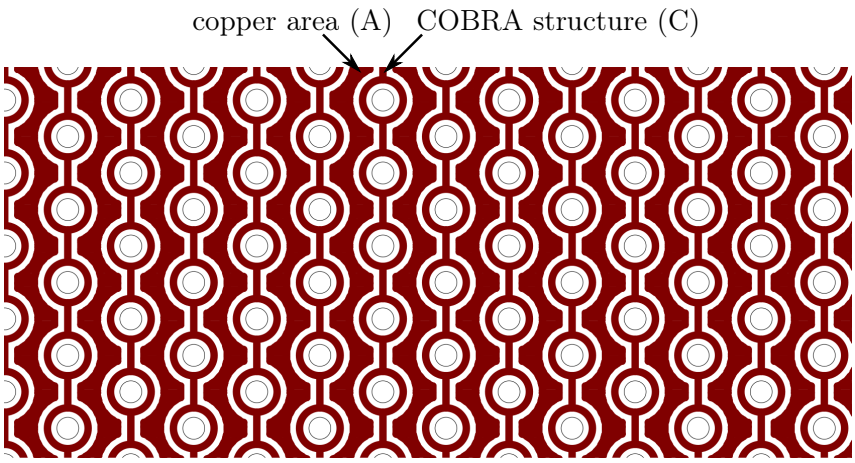

Figure 2.1: COBRA structure of the GEM, the copper layer is depicted in red and the black circles are the GEM holes

1.4). If one applies $\Delta U_{\mathrm{AC}} > 0\,\mathrm{V}$ however, the field changes as seen in fig. 2.4. At $\Delta U_{\mathrm{AC}} = 400\,\mathrm{V}$ most of the field lines end at the top side of the GEM which should improve the IBF suppression since more ions are forced to drift towards the upper surface. Hence the expected IBF is lower at $\Delta U_{\mathrm{AC}} > 0\,\mathrm{V}$. The to investigate the behaviour of the IBF at varying ΔU_{AC} is a key goal of this experiment.

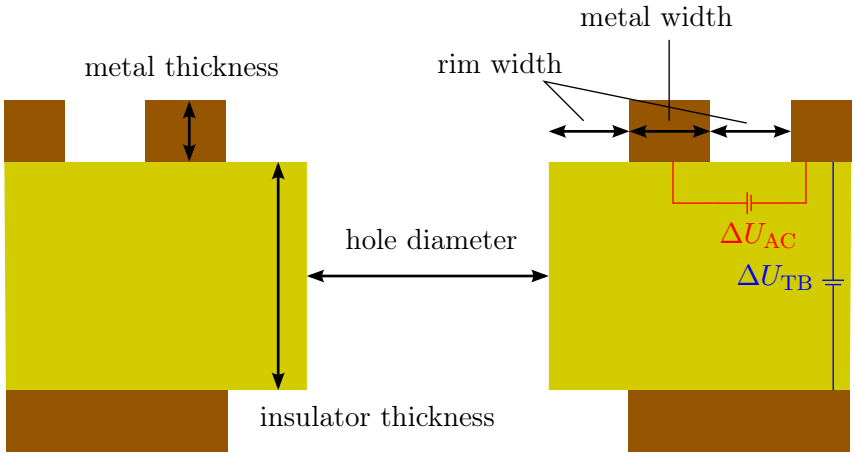

Figure 2.2: Cross section of a COBRA GEM

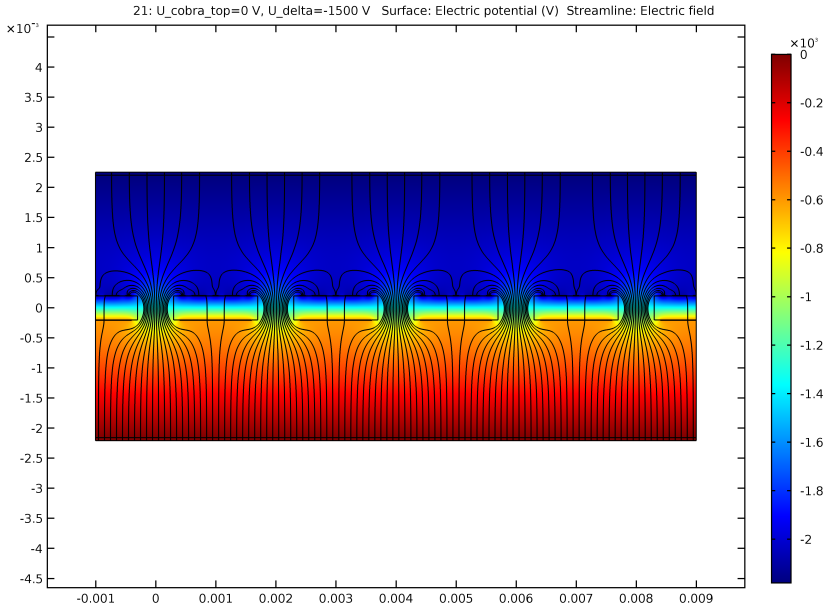

Figure 2.3: Cross section of the COBRA GEM with field line configuration at $\Delta U_{\mathrm{AC}} = 0\,\mathrm{V}$, the field lines are black and the potential is colored

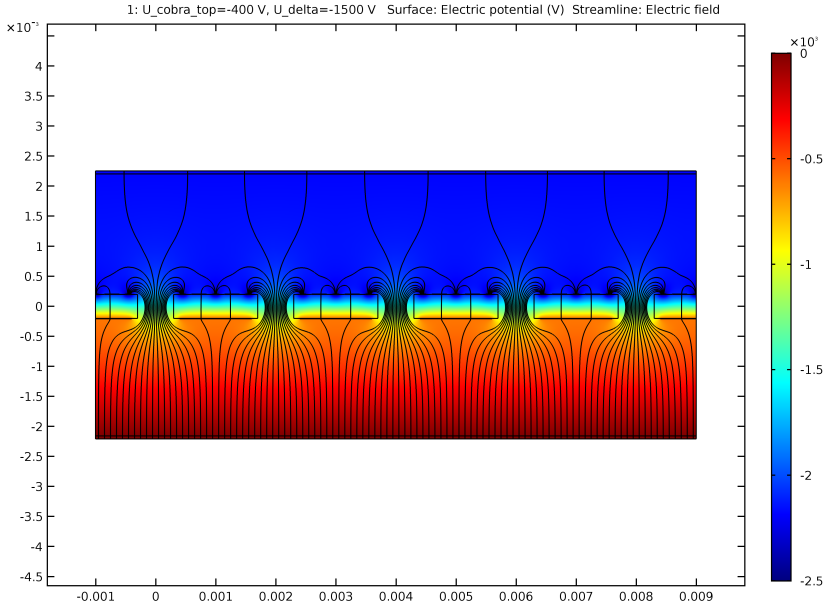

Figure 2.4: Cross section of the COBRA GEM with field line configuration at $\Delta U_{\mathrm{AC}} = 400\,\mathrm{V}$, the field lines are black and the potential is colored

2.2 Design of the COBRA GEM

The COBRA GEM was designed with Eagle, a PCB layout software. In the first version the supply lines for the COBRA structure were kept rather long (see fig. 2.5 and 2.6). However, during functionality tests small remnants of copper on some COBRA GEM specimens lead to sparks between the supply line and the surrounding copper area. These sparks limit the ΔU_{AC} to several volts. For possible future studies on COBRA GEMs, the layout was changed as shown in fig. 2.7 and 2.8 to minimize the probability of sparking remnants. As mentioned above, the bottom side of the GEM has no COBRA structure 2.9. In this experiment a version 1 COBRA GEM was used.

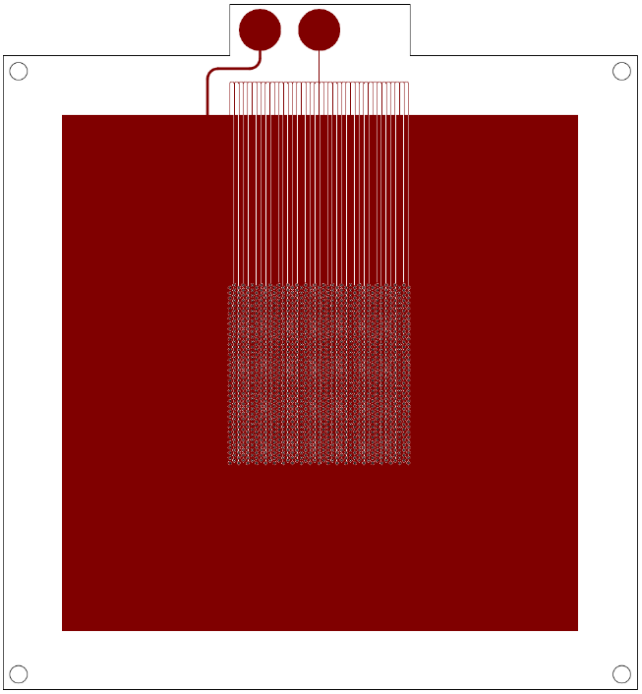

Figure 2.5: Top side of a COBRA GEM version 1

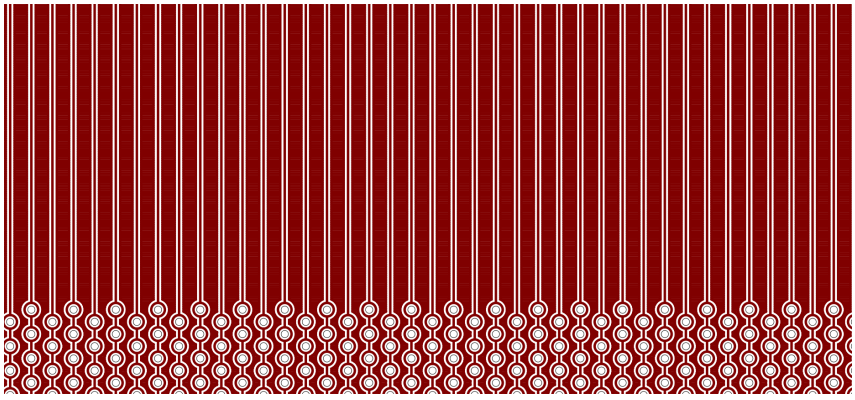

Figure 2.6: Long supply lines of COBRA GEM version 1

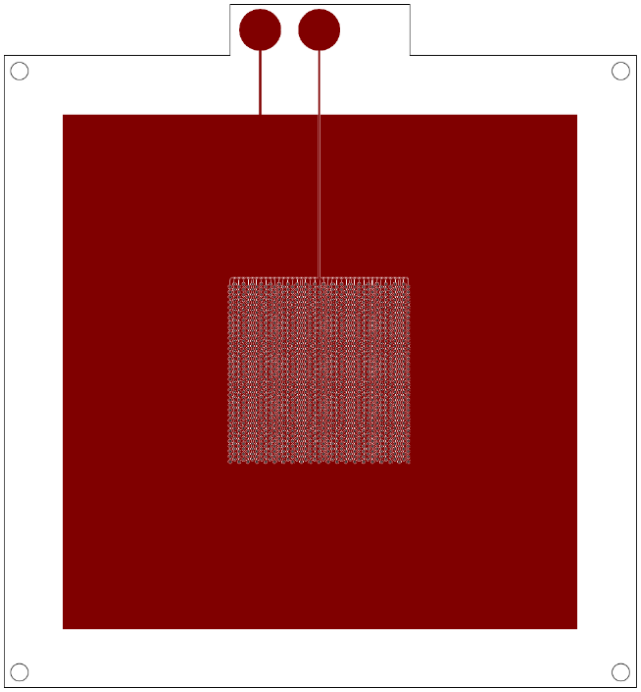

Figure 2.7: Top side of a COBRA GEM version 2

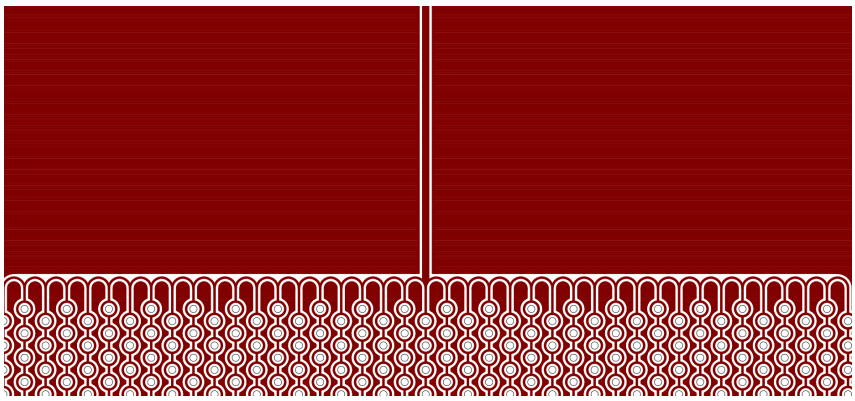

Figure 2.8: The supply lines were shortened in version 2.

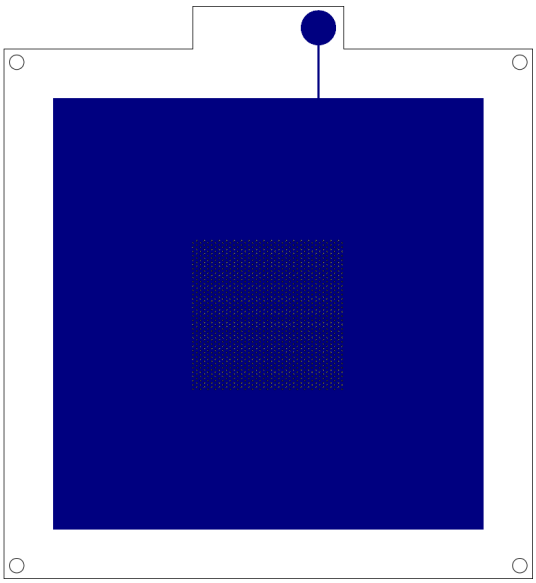

Figure 2.9: The Bottom side of the COBRA GEM has no COBRA structure and is the same for version 1 and 2

Chapter 3

Experiment

In the following chapter the measurement setup that was used to determine the IBF and the effective gain of the COBRA GEM as well as some preparations to do so are discussed. The IBF is defined as:

$$\mathrm{IBF} = \frac{I_\mathrm{C}}{I_\mathrm{A}} \tag{3.1}$$

The following abbreviations will be used throughout the next chapters:

U_Cat : Voltage applied to the cathode
U_C : Voltage applied to the COBRA structure on the top side of the GEM
U_A : Voltage applied to the large area electrode on the top side
ΔU_AC : $U_\mathrm{A} - U_\mathrm{C}$
U_T : Voltage applied to the top side of the GEM when $\Delta U_\mathrm{AC} = 0\,\mathrm{V}$
U_B : Voltage applied to the bottom side of the GEM
ΔU_TB : $U_\mathrm{B} - U_\mathrm{A}$
I_C : Current at the cathode
I_A : Current at the anode
I_prim : primary current

In the experiment only negative currents were measured however positive currents will be plotted for a better readability instead. Only for the calibration of the pico ampere meter negative currents will be used since this is mandatory for a correct calibration.

3.1 Detector setup

The detector is housed in a cast iron casing with windows of mylar foil on every side except the bottom. Inside this casing the anode is fixed to a ground plate with four PVC pillars on which the cathode is mounted in a distance of 37 mm from the anode.

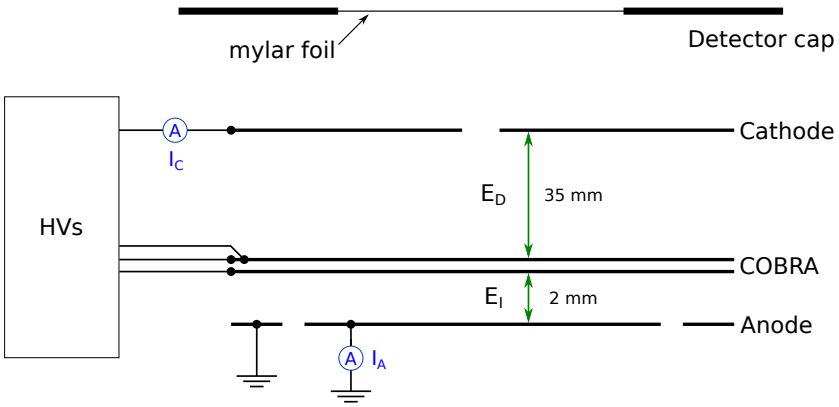

Figure 3.1: A schematic drawing of the detector setup where E_D denotes the drift gap while E_I denotes the induction gap.

A hole is drilled in the middle of the cathode to allow for a better irradiation of the drift volume. The COBRA GEM is fixed on the anode with a 2 mm gap to the anode. With a power supply one can apply potentials to the cathode, the bottom side of the GEM as well as to both electrodes on the top side via SHV coaxial cables. The anode, which is segmented in two parts, is read out using a LEMO coaxial cable. However only the inner part is read out since the outer part is only a small rim where close to no electrons are collected. The currents on the cathode were measured by a pico ampere meter while the anode currents were measured with a Keithley 6517b (Keithley). A scheme of the detector is shown in fig. 3.1. The field between cathode and top side of the GEM is called drift field, the field between bottom side of the GEM and anode is called induction field.

The detector was operated at a drift field of 400 $\frac{\mathrm{V}}{\mathrm{cm}}$ and an induction field of 3 $\frac{\mathrm{kV}}{\mathrm{cm}}$ at different gains. To vary the gain ΔU_TB has to be changed. Therefore U_B was fixed at $-600\,\mathrm{V}$ and U_Cat was adjusted with respect to the change of U_T to maintain the desired drift field. This makes the ions drift towards the cathode and the electrons drift towards the GEM. The chosen gas mixture was $\mathrm{Ar}/\mathrm{CO_2}$ in a mixture of 90 % Ar and 10 % $\mathrm{CO_2}$.

The active volume of the detector was irradiated with a 5 MBq ^{55}Fe-source emitting 5.9 keV gamma rays. Argon has a K-shell energy $E_\mathrm{K} = 3.2\,\mathrm{keV}$ and a L-shell energy $E_\mathrm{L} = 0.3\,\mathrm{keV}$ thus the average energy needed to generate primary charges is $W_\mathrm{i} = 28.8\,\mathrm{eV}$. Therefore there are three scenarios.

a) K absorption + Auger electron

In this case the gamma ray knocks out an electron of the K-shell ($E_e = 2.7\,\text{keV}$) and an Auger electron is emitted from the Ar atom ($E_{\text{Auger}} = 3.2\,\text{keV}$). Those electrons then ionize the gas in the detector and thus create primary electrons. This process contributes to the 5.9 keV peak.

b) K absorption + X-ray

Like in case a) an electron of the K-shell gets knocked out of the atom with $E_e = 2.7\,\text{keV}$. However no Auger electron is emitted in this scenario but instead a γ_{KL} with $E_{\gamma_{\text{KL}}} = 2.9\,\text{keV}$ from the K-L transition and a γ_{LM} with $E_{\gamma_{\text{LM}}} = 0.3\,\text{keV}$ from the following L-M transition are emitted. The 2.9 keV gamma ray can escape the detector without producing primary electrons. The γ_{LM} and the electron create the 3.0 keV peak by ionizing gas molecules in the detector.

c) L absorption + X-ray

Here an electron of the L-shell gets knocked out of the Ar atom ($E_e = 5.6\,\text{keV}$). Subsequently a γ_{LM} with $E_{\gamma_{\text{LM}}} = 0.3\,\text{keV}$ from the L-M transition is emitted. The electron and the γ_{LM} create electron-ion pairs in the drift volume. Just like in case a) this adds to the 5.9 keV peak in the spectrum (see fig. 3.3).

One has to keep in mind that the counting rate of the detector is not equal to the activity of the radiation source.

3.2 Determination of the primary current

Among other properties the effective gain of a COBRA GEM was studied in this work. It is defined as in equation 1.3. In order to determine G_{eff} it is necessary to identify the primary current I_{prim}.

3.2.1 Source on top of the detector

In a first attempt to determine the primary current, the iron source was placed outside of the detector housing at one of the mylar windows (see fig. 3.2). The energy spectrum was recorded with a FAST ComTec MCA4 multichannel analyzer (MCA). For that purpose the following voltages were applied leading to an effective gain in the order of 10000:

$$\begin{aligned} U_{\text{Cat}} &= -3600\,\text{V} \\ U_{\text{T}} &= -2220\,\text{V} \\ U_{\text{B}} &= -600\,\text{V} \end{aligned}$$

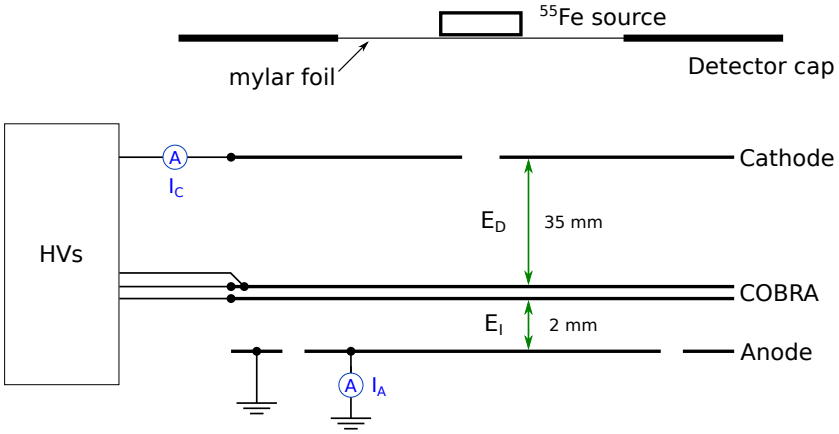

Figure 3.2: A schematic drawing of the detector setup where E_D denotes the drift gap while E_I denotes the induction gap. The source is placed outside the detector housing on top of the detector.

The signal from the anode was amplified with a charge sensitive preamplifier (ORTEC 142) and transferred to a shaper (ORTEC 474 Timing Filter Amplifier) which integrates and differentiates the signal to suppress the noise and form it for a better digitization with the MCA while preserving the energy pulse-hight relation. The obtained energy spectrum is shown in fig. 3.3.

The ADC channels on the x-axis represent different energies of the spectrum, i.e. the higher the number of the channel, the higher the energy. The number of counts is drawn on the y-axis. On the left side of the spectrum one can see the noise which can be fitted by an exponential function. The peak in the middle is the escape peak which corresponds to 3.0 keV (3.1 b)) while the bigger peak corresponds to 5.9 keV (3.1 a) and c)). The primary current is proportional to the counting rate:

$$I_\mathrm{prim} = \frac{e}{W_\mathrm{i}} \cdot (R_{3.0} \cdot 3.0\,\mathrm{keV} + R_{5.9} \cdot 5.9\,\mathrm{keV}) \tag{3.2}$$

where e is the elementary charge, W_i is the work function and $R_{3.0}$ and $R_{5.9}$ are the counting rates of the individual energies. $R_{3.0}$ and $R_{5.9}$ were determined by fitting the energy spectrum with the sum of two gaussian functions and an exponential function for the noise. A gaussian function is defined as:

$$f(x) = a \cdot e^{-\frac{(x-b)^2}{2c^2}} \tag{3.3}$$

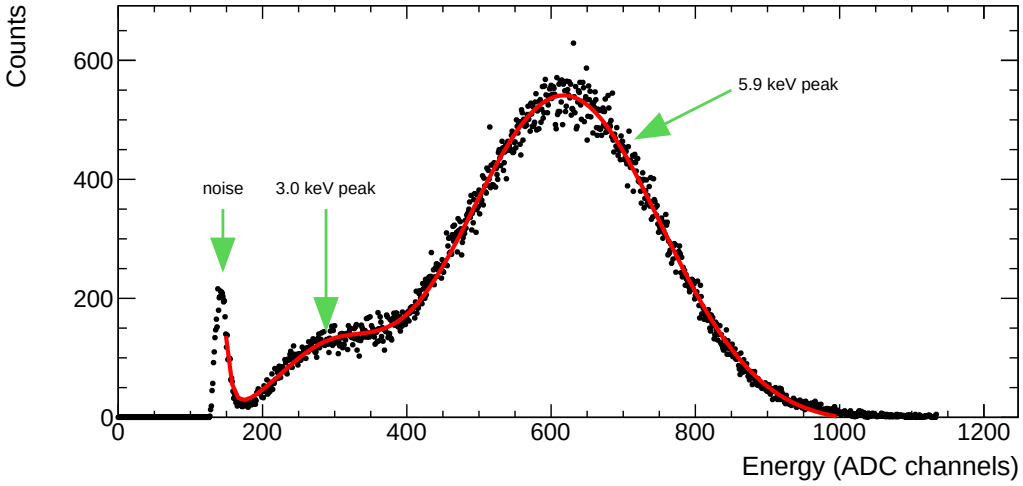

Figure 3.3: Energy spectrum obtained with the ^{55}Fe source outside on top of the detector

The Rate R is the integral over the corresponding gaussian function divided by the measuring time. The integral is defined as:

$$\int_{-\infty}^{+\infty} a \cdot e^{-\frac{(x-b)^2}{2c^2}} dx = a\sqrt{2\pi c^2} \tag{3.4}$$

With the resulting parameters from the fit and equation 3.4 we obtain $R_{3.0} \approx 150\,\mathrm{Hz}$ and $R_{5.9} \approx 1.4\,\mathrm{kHz}$. Therefore

$$I_{\mathrm{prim}} \approx 0.05\,\mathrm{pA}.$$

With an ion back flow in the range of about 50 % to 15 % as shown later, the current at the cathode would be in the order of 10 pA. Currents at this magnitude are very difficult to measure as they are close to the lower detection threshold of our current meters. However the energy resolution of the COBRA GEM could be determined with this setup:

$$\frac{\Delta E}{E} = 21.8(1)\,\%$$

3.2.2 Source on top of the cathode

In order to get a higher primary current, the radiation source was placed inside the detector housing directly on top of the cathode (see fig. 3.4).

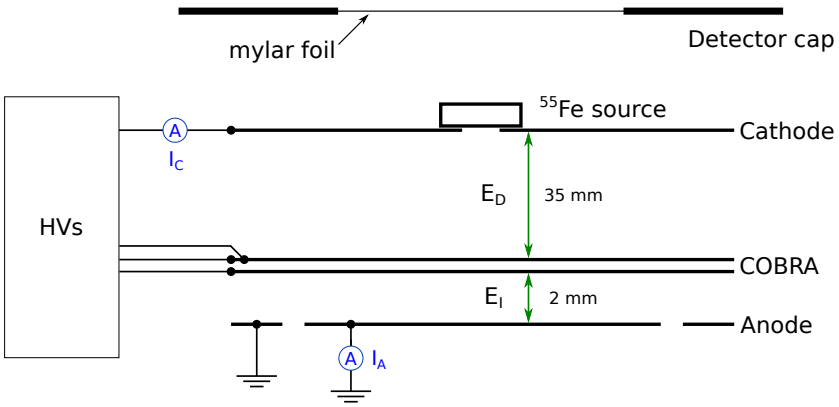

Figure 3.4: A schematic drawing of the detector setup where E_D denotes the drift gap while E_I denotes the induction gap. The source is placed inside the detector housing on top of the cathode.

Again the spectrum was recorded to determine the rate in order to calculate the primary current. But as one can see in fig. 3.5 the spectrum looks quite different from the one in fig. 3.3. The escape peak is merged with the 5.9 keV peak which makes it impossible to calculate the rates $R_{3.0}$ and $R_{5.9}$ separately. Additionally one can see another peak at higher energies than 5.9 keV which is caused by pileup in the preamplifier. The preamplifier gathers charge from the anode and is discharged by a resistor while the signal transferred to the shaper is the voltage drop at the resistor. However the charge goes down exponentially with respect to time since the preamplifier and the resistor form a RC element. With this setup the rate is too high for the preamplifier to fully discharge before the next event charges it up again. Hence the signal which is proportional to the charge is then higher than it actually should be. Considering this one can identify the right peak in the spectrum as a double 5.9 keV event because it is at about double the ADC channel number as the merged peak.

As the determination of the primary current by fitting the energy spectrum was not possible anymore the primary current had to be measured directly. Therefore two options were chosen to confirm the result. A first measurement with the following voltages was conducted:

$$\begin{aligned} U_\mathrm{Cat} &= -1380\,\mathrm{V} \\ U_\mathrm{T} &= 0\,\mathrm{V} \\ U_\mathrm{B} &= 0\,\mathrm{V} \end{aligned}$$

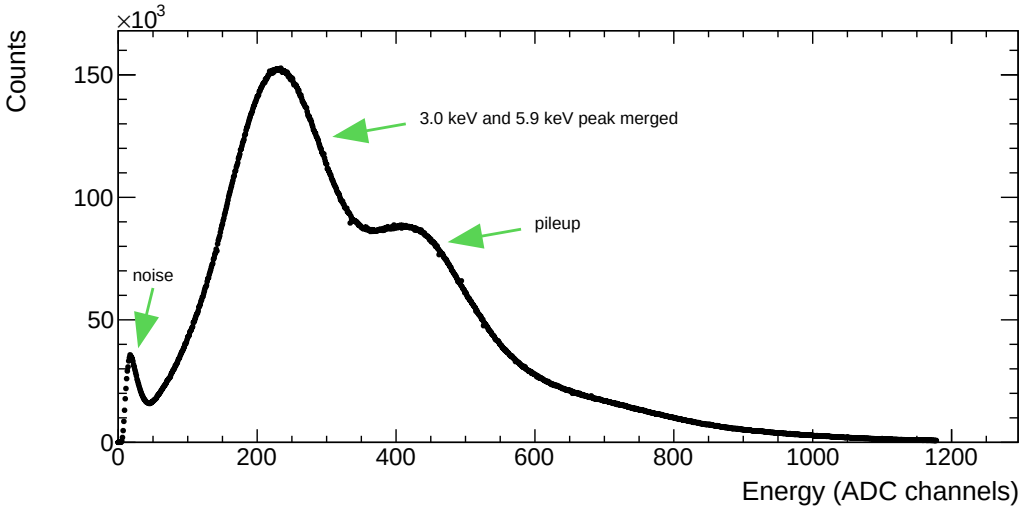

Figure 3.5: Energy spectrum obtained with the ^{55}Fe source inside the detector housing on top of the cathode

The current was measured hereby at the top side of the GEM. Both electrodes on the top side were shorted for this purpose. After that a measurement with the second configuration was done:

$$U_{\mathrm{Cat}} = 0\,\mathrm{V}$$
$$U_{\mathrm{T}} = -1380\,\mathrm{V}$$
$$U_{\mathrm{B}} = -1380\,\mathrm{V}$$

Here the cathode was read out. In both cases the Keithley was used to perform the current measurement. The following results were obtained:

$$I^1_{\mathrm{prim}} = 19.6(3)\,\mathrm{pA}$$
$$I^2_{\mathrm{prim}} = 19.8(4)\,\mathrm{pA}$$

Both measurements are equal in the range of uncertainty. For further calculations the mean of those two measurements is used.

$$I_{\mathrm{prim}} = 19.7(3)\,\mathrm{pA}$$

3.3 Charge up

One big source of systematical errors for the current measurements at the anode and the cathode is the charge up of the insulator of the COBRA GEM. Especially the

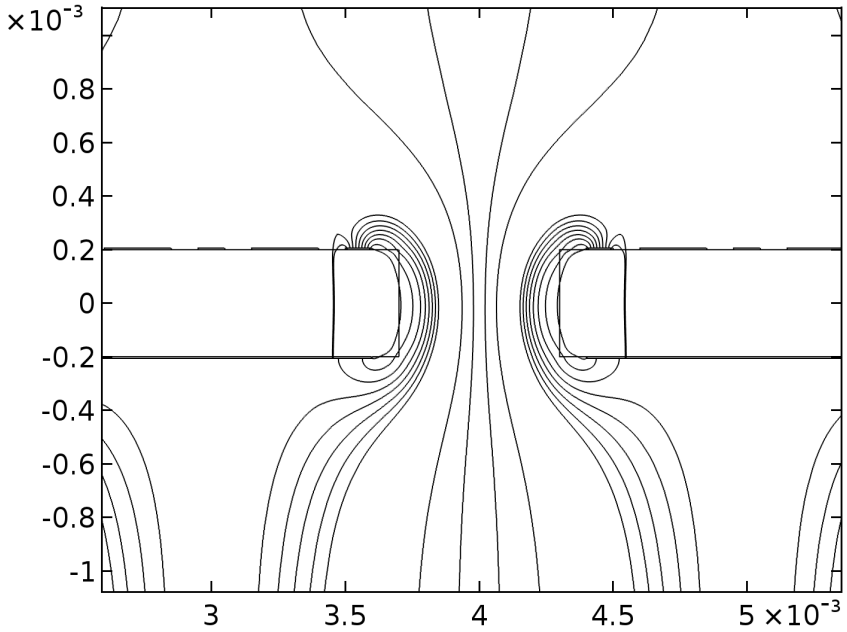

Figure 3.6: Cross section of the GEM with simulated field lines at $\Delta U_{\mathrm{TB}} = 1400\,\mathrm{V}$ and $\Delta U_{\mathrm{AC}} = 0\,\mathrm{V}$

gain measurements are affected by this phenomenon. As one can see in fig. 3.6 some field lines lead to the insulator and not to a copper area and therefore electrons, especially from the avalanche amplification, can reach the insulator where they are stopped and diffuse slowly to their respective electrode. This undesired behaviour of the electrons leads to the insulator charging up and thus an amplification of the gain. The impact on the gain can be seen in the green and blue curve in fig 3.7 since these measurements were started with an uncharged COBRA GEM. The initial charge up takes about 15 h at $\Delta U_{\mathrm{TB}} = 1350\,\mathrm{V}$ but even after that period of time one can not be sure if the gain stays constant. At $\Delta U_{\mathrm{TB}} = 1400\,\mathrm{V}$ the initial charge up is not completed within 24 h. The amplification of the gain during this period qualitatively coincides with the observations made by [9]. In the red curve in fig. 3.7 one can identify four significant and numerous smaller jumps in the current measurement. The significant ones are assumed to be a result of an excessive charge density in at least one GEM hole because of the charged up insulator. The jump in the measurement appears when a spark disrupts between the top and the bottom side of the GEM. Assumingly thereby the insulator at least partly discharges and the positive effect of the charge up on the gain is decreased to some extent. The smaller

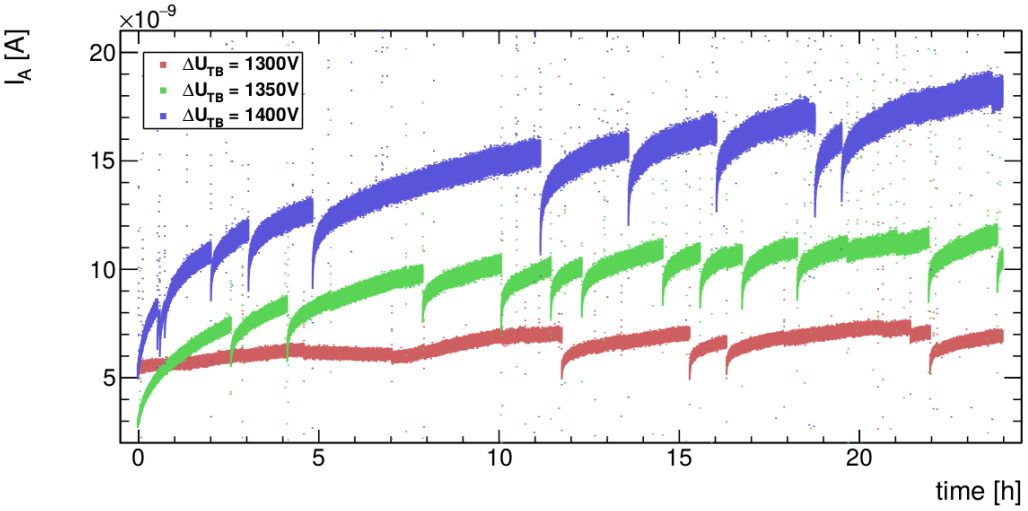

Figure 3.7: Current measurement plotted as a function of time at $\Delta U_{\mathrm{TB}} = 1300\,\mathrm{V}$ (red), $\Delta U_{\mathrm{TB}} = 1350\,\mathrm{V}$ (green) and $\Delta U_{\mathrm{TB}} = 1400\,\mathrm{V}$ blue). The measurement for the green and blue curve were started with an uncharged GEM. Therefore the initial charge up can be observed.

jumps are possibly the result of shorts of the GEM when the charge density in a single hole gets too high occasionally. This maybe happens when numerous primary electrons reach the same hole in the GEM. It may also be that a small jump results from a spark between the insulator and the bottom side of the COBRA GEM due to high charge density in a hole.

Comparing the three curves in fig. 3.7 it is hard to identify any tendencies about the behaviour of the discharges. On the one hand the number of significant discharges more that doubles when changing ΔU_{TB} from 1300 V to 1350 V which could be caused by a faster charge up of the insulator caused by the higher number of generated electrons in an avalanche at higher ΔU_{TB}. On the other hand the number of significant discharges stays the same when switching ΔU_{TB} from 1350 V to 1400 V. This seems to be contradictory. Hence the steeper slope of the blue curve compared to the green is probably a result of G_{eff} increasing exponentially as a function of ΔU_{TB}. The distances between the significant jumps seem to be randomly distributed and they appear at different gains. However, it seems that the gain drops by 25 % after each discharge with respect to its value before the discharge. In the 15 min measurements of the current that were executed it was not possible to know whether the measurement was on the low or the high end of the gain. Therefore a

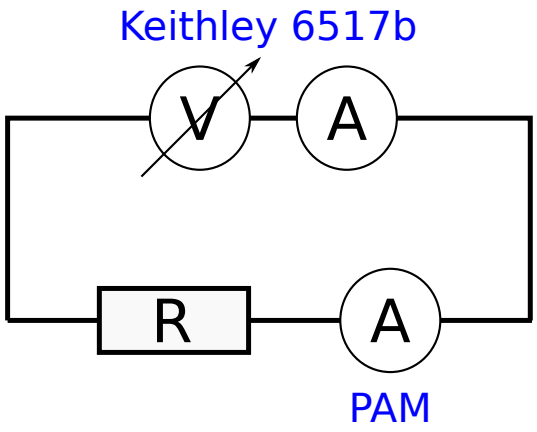

Figure 3.8: A schematic drawing of the calibration setup where the Keithley is used to apply a potential and to measure the current

systematic error of

$$\Delta I = I^{+33\,\%}_{-25\,\%}$$

is applied since the measured value can as well be 25 % lower or 33 % higher. This error, however, only influences the gain measurement but not the ion back flow measurements because the discharges affect I_C and I_A similarly.

Altogether these charge up effects with the corresponding discharges are not well understood and should be investigated further. Similar effects were observed by [10].

3.4 Calibration of the pico ampere meter

Up to this point every current measurement was performed with the Keithley. To measure the ion back flow, two ampere meters were needed since I_A and I_C were to be measured simultaneously. The current at the cathode was measured with a pico ampere meter. Since the PAM has four measurement ranges (see table 3.1) a rough estimation of the expected currents at the cathode had to be done. For the upper limit $G_{\text{eff}} = 10^4$ and IBF = 0.5 were assumed. With equation (1.3) and 3.1 and the measured I_{prim}, this leads to $I_C \approx 100\,\text{nA}$. The lower value was estimated to be $I_C \approx 100\,\text{pA}$ using $G_{\text{eff}} = 500$ and IBF = 0.01. Therefore mode 2 and 3 of the PAM had to be calibrated.

To obtain a calibration, a simple circuit consisting of the Keithley, the PAM and a resistor, where the Keithley served as a voltage source as well as to measure a reference current, was used (see fig 3.8). The PAM and the Keithley measured

mode	range
0	10 mA
1	100 µA
2	1 µA
3	10 nA

Table 3.1: Measurement modes of the PAM

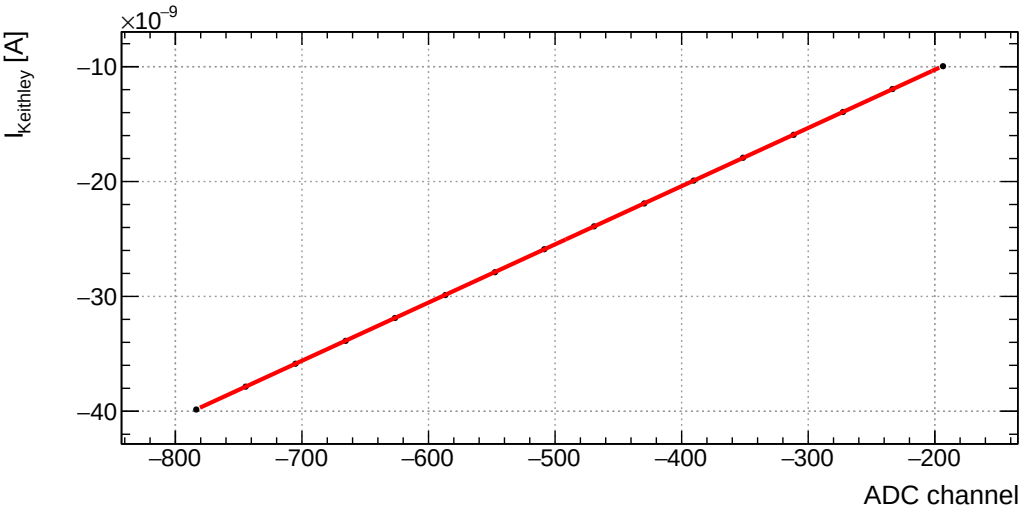

Figure 3.9: The Keithley measurement plotted as a function of the corresponding ADC channel with linear fit (red) to get the calibration parameters for the PAM mode 2

the current so it could be determined how much the values from the PAM and the Keithley vary. A current scan was performed by varying the voltage drop over the resistor. Since the measurements were performed from −10 pA to almost −40 nA two different resistors were used to avoid applying voltage drops in the order of 1 mV. Fluctuations of the voltage source lead to unnecessarily big uncertainties of the current measurements at that scale. The utilized resistors had a resistance of 500 MΩ and 10 GΩ.

The actual output of the PAM is the current in units of ADC channels. The calibration of the PAM consists of two parameters. A slope and an offset which then are used to assign a certain current to the ADC channels according to the following

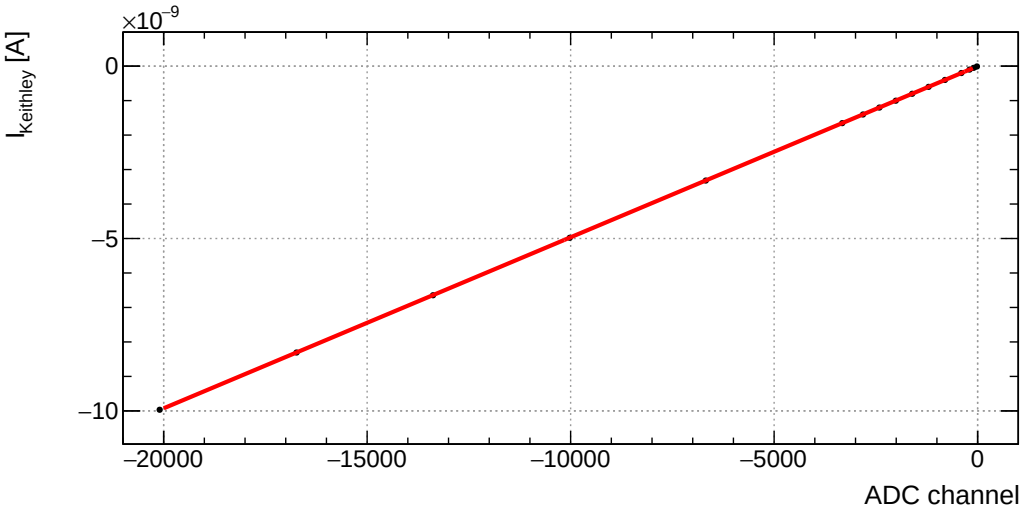

Figure 3.10: The Keithley measurement plotted as a function of the corresponding ADC channel with linear fit (red) to get the calibration parameters for the PAM mode 3

equation:

$$I = (ADC - t) \cdot s \tag{3.5}$$

with I being the current, ADC the measured ADC channel, t the offset and s the slope. To obtain t and s, the current measured by the Keithley was used as a reference and plotted as a function of the ADC channels. Then a linear fit was applied (see fig. 3.9 and 3.10). The received slope and offset were used for the calibration.

The Calibration was tested by repeating the measurements and plotting the difference between the Keithley and the PAM measurement over the Keithley measurement for mode 2 and 3 (see fig. 3.11 and 3.12). The variation of the PAM measurement from the Keithley measurement will be taken into account as a systematical error. Fig. 3.13 is a zoomed-in version of fig. 3.12 for a better visibility of the region of interest. I_C is in a range of $-300\,\text{pA}$ to $-2\,\text{nA}$ in the IBF measurements for variable ΔU_{AC}. In the IBF measurements for $\Delta U_{AC} = 0\,\text{V}$ I_C goes up to $-16\,\text{nA}$. A difference of $\approx 1.4\,\%$ from $-12\,\text{nA}$ to $-16\,\text{nA}$ leads to a systematical error in the order of 10^{-10} at IBF in the order of 10^{-1} at mode 2. With a difference of $\approx 0.27\,\%$ from $-200\,\text{pA}$ to $-1\,\text{nA}$ and under $0.1\,\%$ from $-1.7\,\text{nA}$ to $-8\,\text{nA}$ the calibration for mode 3 leads to a systematical error in the order of 10^{-13} at IBF in the order of 10^{-1} at IBF measurements with variable ΔU_{AC}.

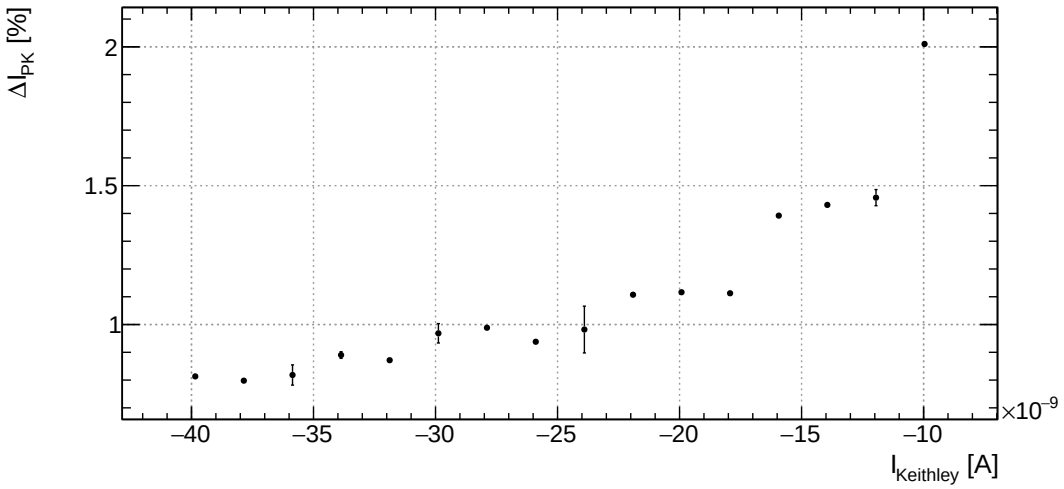

Figure 3.11: Variation of the PAM measurement from the Keithley measurement plotted as a function of the Keithley measurement for PAM mode 2

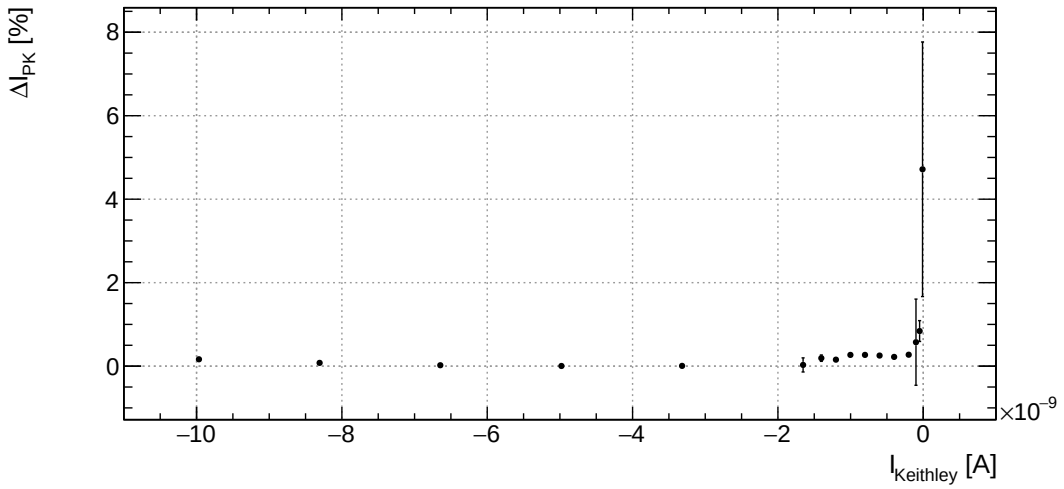

Figure 3.12: Variation of the PAM measurement from the Keithley measurement plotted as a function of the Keithley measurement for PAM mode 3

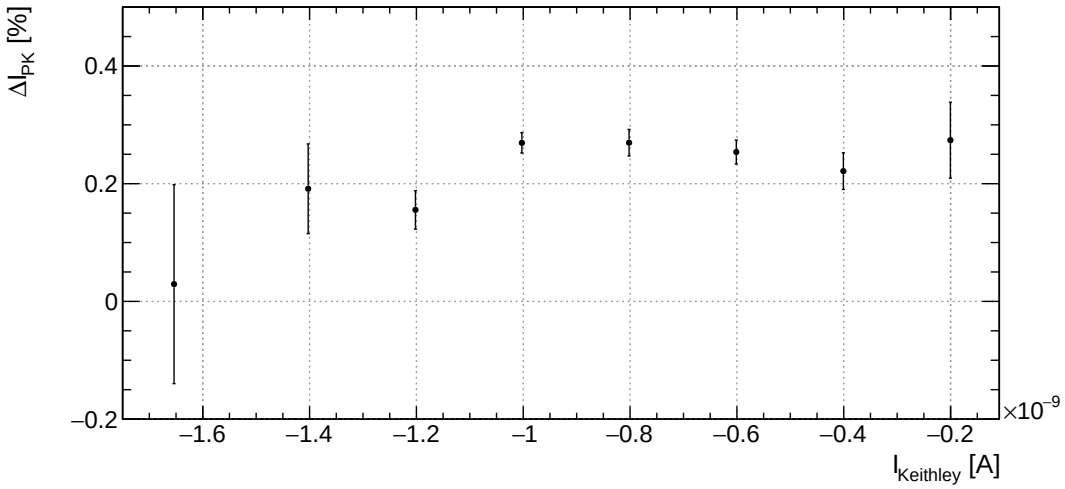

Figure 3.13: Variation of the PAM measurement from the Keithley measurement plotted as a function of the Keithley measurement for PAM mode 3, zoomed in to the region of interest

Chapter 4

Results

In this chapter the results concerning the gain and ion back flow measurements are elaborated. To keep the influence of charge up effects as low as possible, the COBRA GEM was operated with the following potentials for about 24 h before the gain measurements were performed:

$$\begin{aligned} U_{\mathrm{Cat}} &= -3380\,\mathrm{V} \\ U_{\mathrm{T}} &= -2000\,\mathrm{V} \\ U_{\mathrm{B}} &= -600\,\mathrm{V} \end{aligned}$$

Hence G_{eff} at $\Delta U_{\mathrm{TB}} = 1400\,\mathrm{V}$ and higher could possibly be higher than the measured value 3.3.

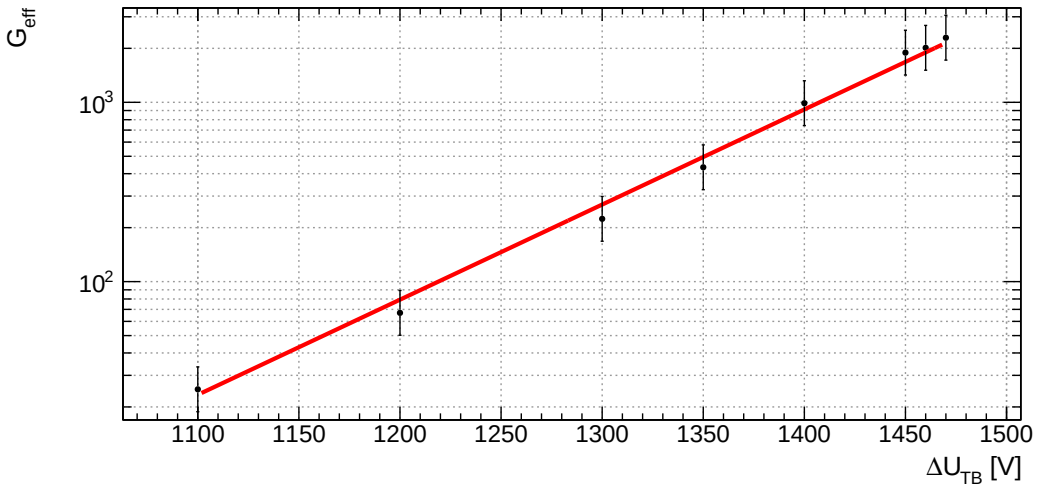

Figure 4.1: Gain as a function of ΔU_{TB} at $\Delta U_{\mathrm{AC}} = 0\,\mathrm{V}$ fitted with an exponential function

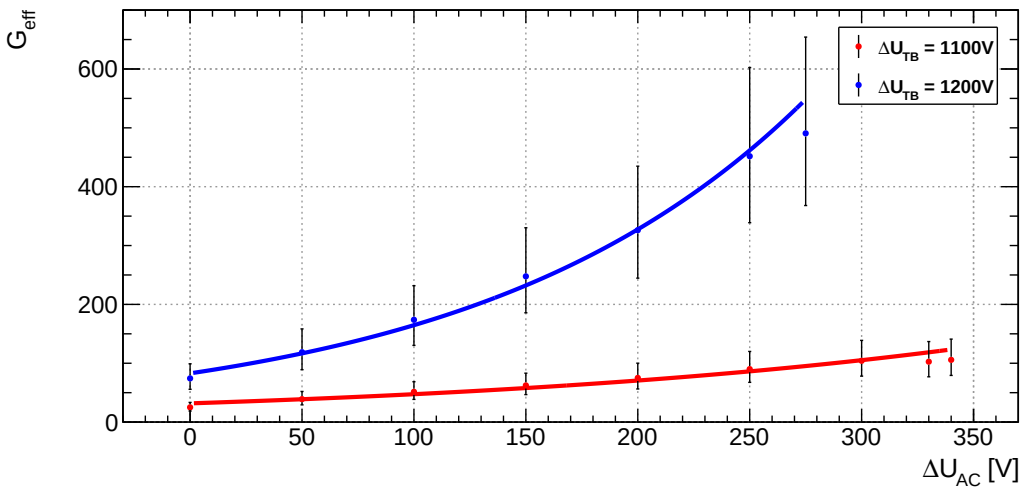

Figure 4.2: Gain as a function of ΔU_{AC} at $\Delta U_{\mathrm{TB}} = 1100\,\mathrm{V}$ (red) and $\Delta U_{\mathrm{TB}} = 1200\,\mathrm{V}$ (blue) each fitted with an exponential function

4.1 Gain

First a gain scan of the COBRA GEM was performed by varying ΔU_{TB}. U_{B} was fixed at $-600\,\mathrm{V}$ and U_{T} was varied from $-1800\,\mathrm{V}$ to $-2070\,\mathrm{V}$ while also changing U_{Cat} respectively to maintain a drift field at $E_{\mathrm{D}} = 400\,\frac{\mathrm{V}}{\mathrm{cm}}$. The result is plotted in fig. 4.1. As expected the gain rises exponentially with higher potential differences between bottom and top side of the COBRA GEM. Thus the COBRA GEM qualitatively behaves like a standard GEM foil when $\Delta U_{\mathrm{AC}} = 0\,\mathrm{V}$ [11]. The $\Delta U_{\mathrm{AC}} = 0\,\mathrm{V}$ gain measurement as expected qualitatively matches the result obtained by [3].

Then the behaviour of the gain when changing ΔU_{AC} was studied. Two measurement series were performed with the setups given in tab. 4.1. Based on that, U_{C} was varied up to $-2040\,\mathrm{V}$ in series 1 and $-2075\,\mathrm{V}$ in series 2. This way the curves in fig. 4.2 were obtained. Series 1 is depicted in red and series 2 in blue while both are fitted with an exponential function (solid line). Seemingly the gain rises exponentially by applying ΔU_{AC}. Qualitatively this is also expected [3]. The large error bars result from the charge up effects of the GEM (see 3.3).

	series 1	series 2
U_{B}	$-600\,\mathrm{V}$	$-600\,\mathrm{V}$
U_{T}	$-1700\,\mathrm{V}$	$-1800\,\mathrm{V}$
U_{Cat}	$-3080\,\mathrm{V}$	$-3180\,\mathrm{V}$
G_{eff}	≈ 25	≈ 70

Table 4.1: Voltage setups and gains at $\Delta U_{\mathrm{AC}} = 0\,\mathrm{V}$ for series 1 and 2

4.2 Ion back flow

In this section the IBF reduction capability of the COBRA GEM is discussed. The current measurements at the cathode, needed to calculate the IBF, were done simultaneously with the gain measurements. Fig. 4.3 shows the results for $\Delta U_{\mathrm{AC}} = 0\,\mathrm{V}$. The extraction efficiency increases with higher gain, thus I_{A} rises faster than I_{C}. This leads to the reduction of the IBF at higher ΔU_{TB}.

As expected, increasing ΔU_{AC} has a much bigger impact (see fig. 4.4) since the potential difference on the top side of the COBRA GEM forces numerous field lines to end on the COBRA structure. Here the IBF could be reduced from $\approx 60\,\%$ to $\approx 15\,\%$ at $\Delta U_{\mathrm{TB}} = 1100\,\mathrm{V}$ and therefore the IBF suppressing effect of the COBRA structure has been confirmed. IBF measurements have been done in the past by [3] with a different setup. A COBRA GEM with half the insulator thickness, hole pitch, hole diameter, rim width and metal width as well as a $NeCO_2$ (90/10) gas mixture were used. Quantitatively the results differ clearly but qualitatively the trend in IBF behaviour is the same. This difference probably results mainly from the better extraction efficiency due to the thinner insulator.

4.3 Outlook

Effective gain and ion back flow suppression of a COBRA GEM were studied in this thesis. As expected from the simulations, the IBF could be reduced by increasing ΔU_{AC} and therefore the positive effect of the COBRA structure on IBF suppression was confirmed.

However, the charge up effects of the insulator have to be investigated further since they heavily influence the gain stability. Also COBRA GEMs with different dimensions can be tested upon their influence on IBF or the performance of the COBRA GEM in general. The insulator thickness has influence on the extraction

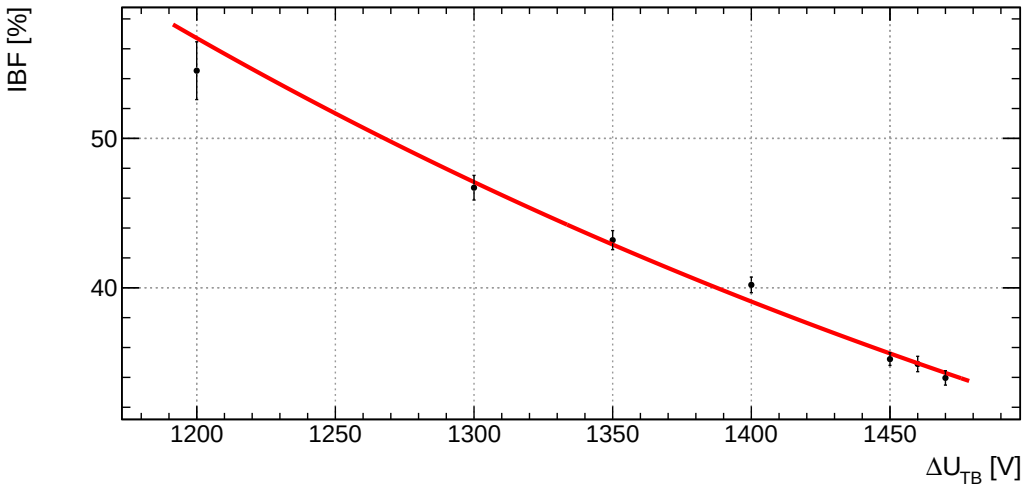

Figure 4.3: Ion back flow as a function of ΔU_{TB} at $\Delta U_{\mathrm{AC}} = 0\,\mathrm{V}$ fitted with an exponential function

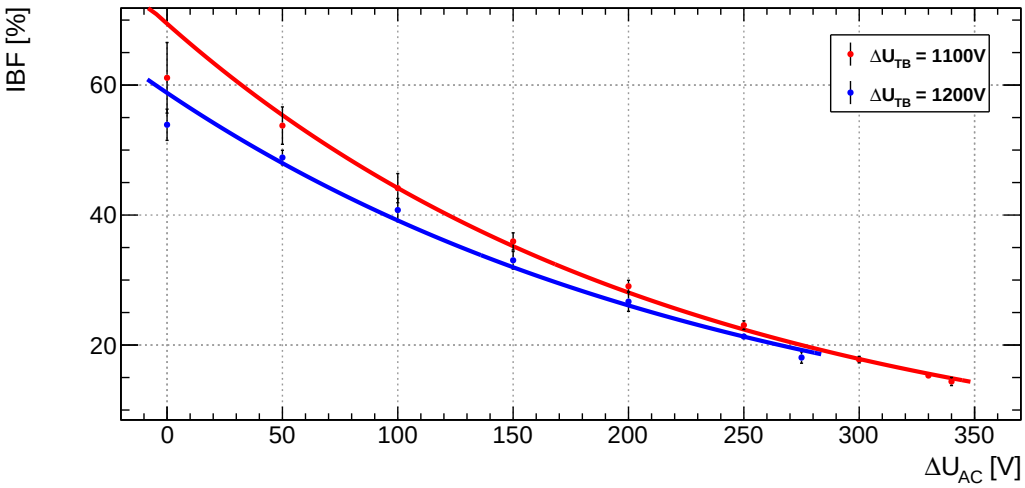

Figure 4.4: Ion back flow as a function of ΔU_{AC} at $\Delta U_{\mathrm{TB}} = 1100\,\mathrm{V}$ (red) and $\Delta U_{\mathrm{TB}} = 1200\,\mathrm{V}$ (blue) each fitted with an exponential function

efficiency and therefore on the gain and the IBF. Also an effect on the charging up of the COBRA GEM has to be expected since a thinner insulator decreases the possibility for electrons to hit the insulator surface. The closer the COBRA structure reaches toward the GEM hole, the fewer field lines end on the surface of the insulator. Therefore an influence of the rim width on the charge up effects is expected. A smaller rim around the holes should reduce the charge up effects. On the other hand a smaller rim is supposed to increase the discharge probability [12]. To find a viable solution for this contradiction further studies have to be carried out.

Appendix A

Pictures of a thick COBRA GEM

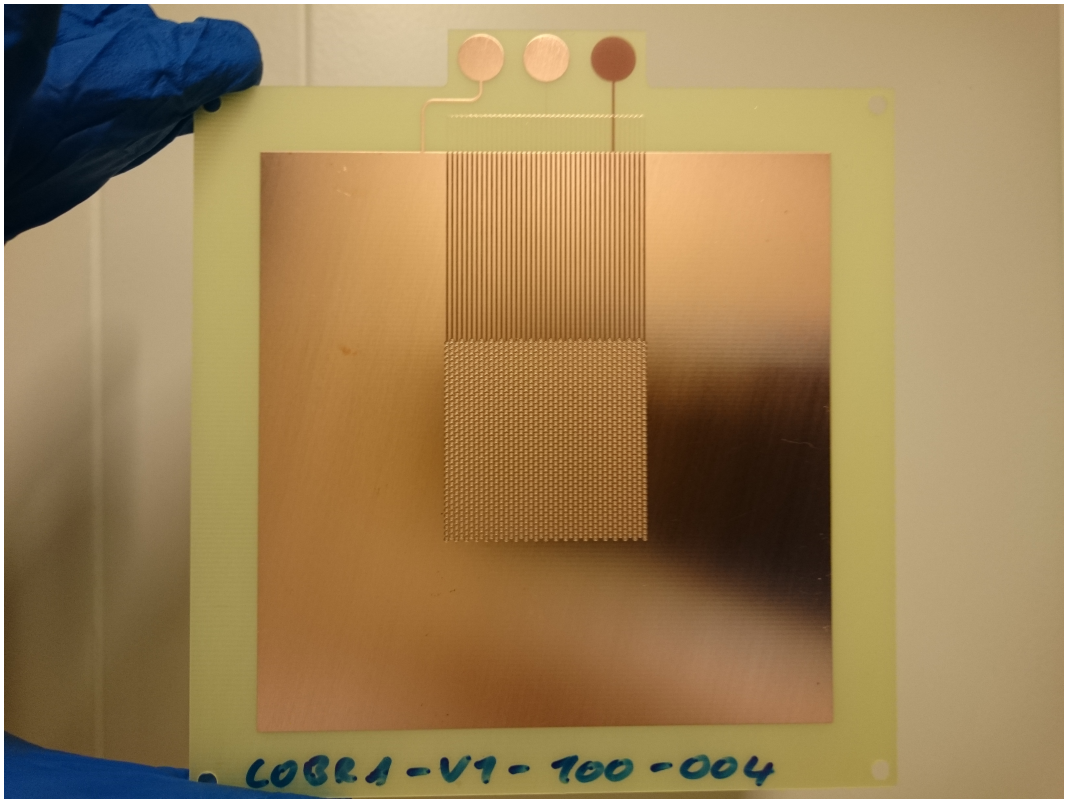

Figure A.1: Picture of the top side of a COBRA GEM similar to the one that was used in this work

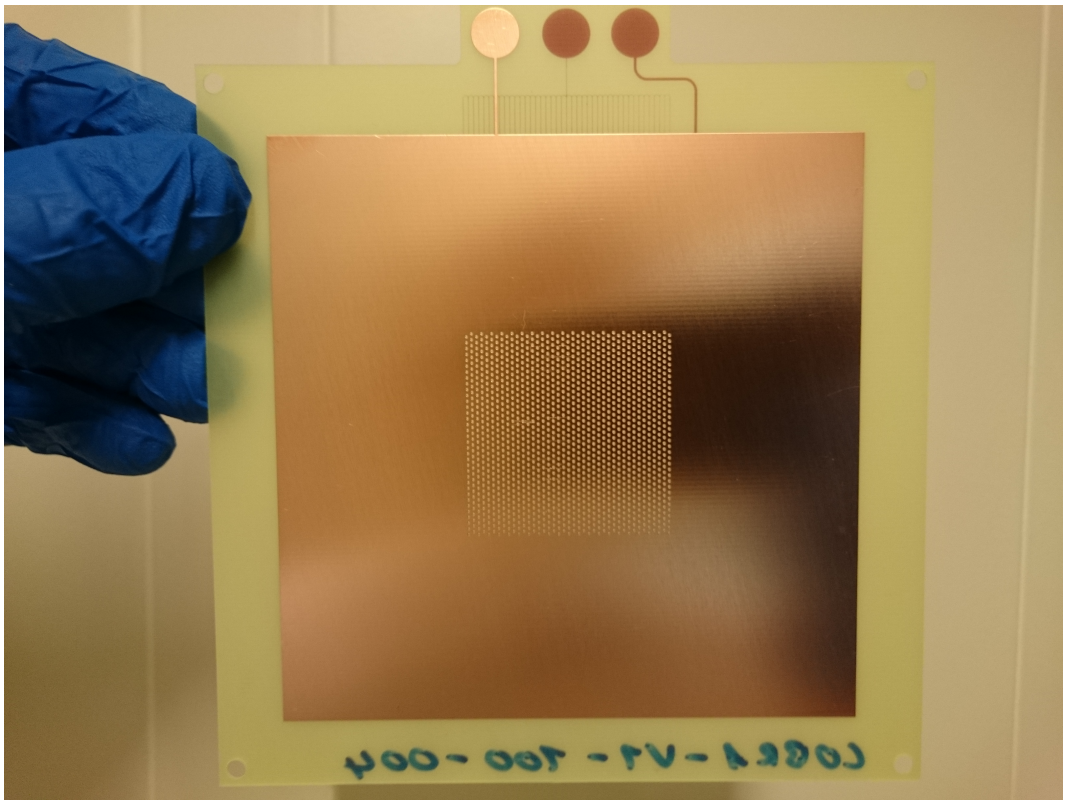

Figure A.2: Picture of the bottom side of a COBRA GEM similar to the one that was used in this work

Appendix B

I_C at IBF measurements

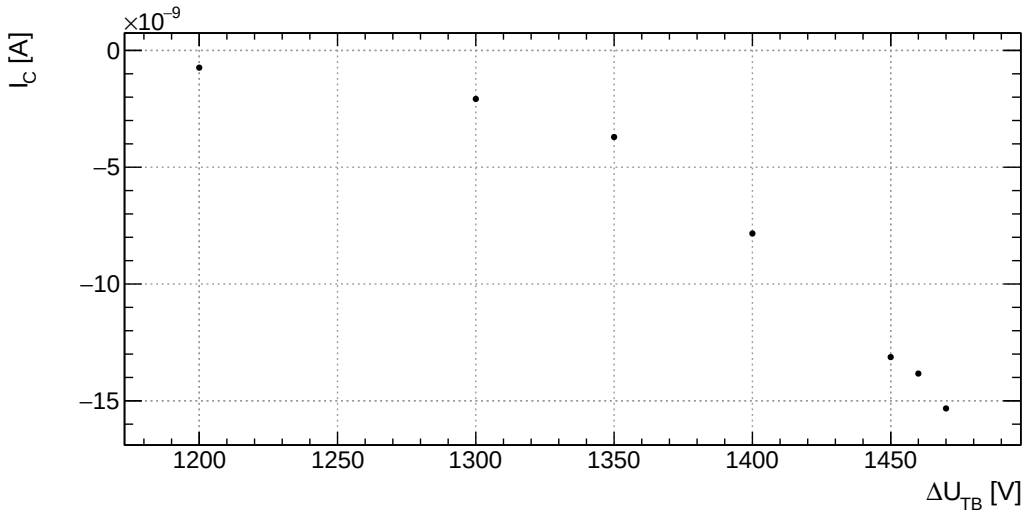

Figure B.1: Pico ampere meter current during IBF measurement at $\Delta U_{\mathrm{AC}} = 0\,\mathrm{V}$

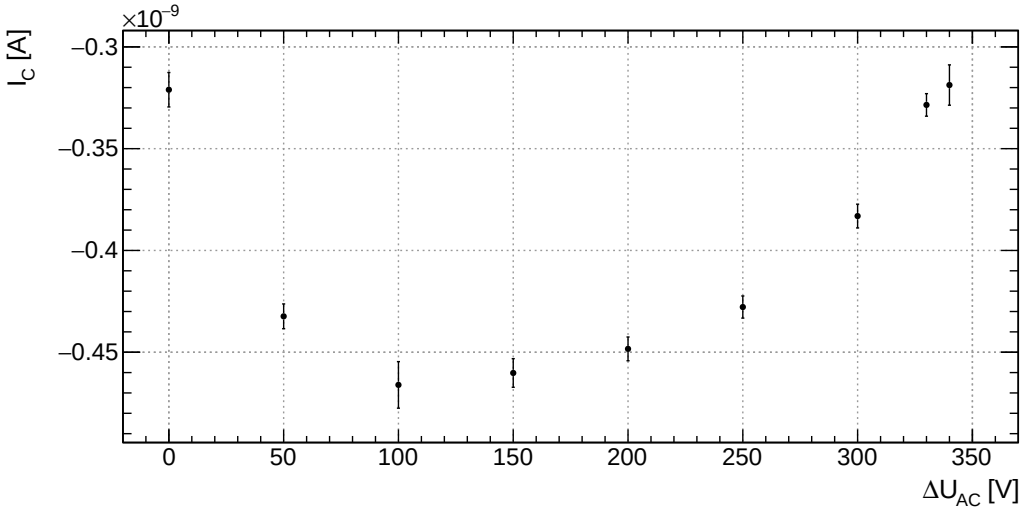

Figure B.2: Pico ampere meter current during IBF measurement at $\Delta U_{\mathrm{TB}} = 1100\,\mathrm{V}$

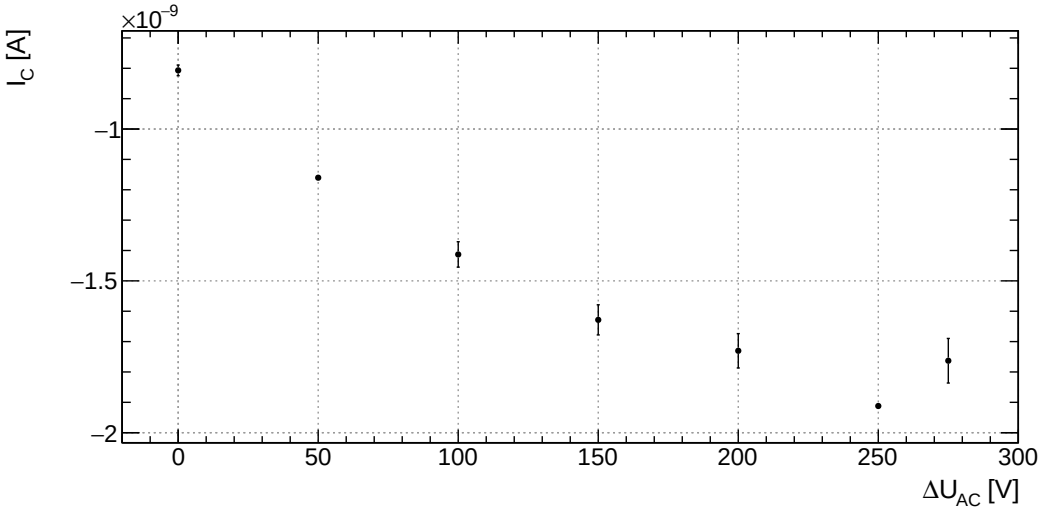

Figure B.3: Pico ampere meter current during IBF measurement at $\Delta U_{\mathrm{TB}} = 1200\,\mathrm{V}$

Bibliography

[1] D.R. Nygren and J.N. Marx. »The Time Projection Chamber«. In: *Physics Today* (Oct. 1978), p. 46.

[2] F. Sauli. »GEM: A new concept for electron amplification in gas detectors«. In: *NIMA* 386 (1997). sauli, gem, gas electron multiplier, pp. 531–534.

[3] K Terasaki. »Study of ion back flow suppression with thick cobra gem«. In: *Journal of Instrumentation* 9.03 (2014), p. C03014. URL: http://stacks.iop.org/1748-0221/9/i=03/a=C03014.

[4] Martin Berger. »Development, Commissioning and Spatial Resolution Studies of a new GEM based TPC«. PhD thesis. Technische Universität München, 26 11 2015.

[5] G. Charpak et al. »The use of multiwire proportional counters to select and localize charged particles«. In: *Nuclear Instruments and Methods* 62.3 (Jan. 1968), pp. 262–268.

[6] J. Alme et al. »The ALICE tpc, a large 3-dimensional tracking device with fast readout for ultra-high multiplicity events«. In: *Nuclear Instruments and Methods in Physics Research Section A: Accelerators, Spectrometers, Detectors and Associated Equipment* 622.1 (2010), pp. 316–367. ISSN: 0168-9002. DOI: http://dx.doi.org/10.1016/j.nima.2010.04.042. URL: http://www.sciencedirect.com/science/article/pii/S0168900210008910.

[7] ALICE collaboration. *Upgrade of the ALICE Time Projection Chamber*. Tech. rep. CERN-LHCC-2013-020. ALICE-TDR-016. TPC upgrade, TPC, Alice. Geneva: CERN, Oct. 2013. URL: https://cds.cern.ch/record/1622286.

[8] *Addendum to the Technical Design Report for the Upgrade of the ALICE Time Projection Chamber*. Tech. rep. CERN-LHCC-2015-002. ALICE-TDR-016-ADD-1. alice, tpc, addendum. Geneva: CERN, Feb. 2015. URL: https://cds.cern.ch/record/1984329.

[9] P. M. M. Correia et al. »A dynamic method for charging-up calculations: the case of GEM«. In: *JINST* 9 (2014), P07025. DOI: 10.1088/1748-0221/9/07/P07025. arXiv: 1401.4009 [physics.ins-det].

[10] P.M.M. Correia et al. *Thick GEM charging up simulation*. Talk at 13th RD51 Collaboration Meeting. July 2014.

[11] Florian Dufter. »Study of propagating discharges in GEM-based detectors«. Technische Universität München, 26 08 2016.

[12] R. Chechnik et al., eds. *Thick GEM-like (THGEM) Detectors and Their Possible Applications*. Mar. 2006.

Danksagung

Zuallererst möchte ich natürlich der Themenstellerin Prof. Laura Fabbietti danken, ohne die es diese Arbeit gar nicht gegeben hätte.

Als nächstes gilt mein besonderer Dank meinem Betreuer Dr. Martin Berger, für die großartige Unterstützung während der gesamten Zeit. Du hast jede meiner Fragen geduldig beantwortet und mir geholfen, wenn ich mal ein paar mehr Hände oder Tipps zum Experiment gebraucht habe. Sogar wenn ich mir manchmal selbst ein bisschen nervig vorkam, hast du dir nie was anmerken lassen. Auch für das Einrichten der PAM-Software und all die Kleinigkeiten die du gemacht hast, die letztendlich einen großen Beitrag zum Gelingen der Arbeit geleistet haben, nochmal ein Dankeschön.

Ebenfalls möchte ich Andreas Mathis danken. Du standst mir stets mit Rat und Tat zur Seite, egal ob es um den Versuch, Administratives oder was sonst noch so alles angefallen ist ging.

Another thanks has to go to Dr. Piotr Gasik. With your expertise in gas detectors I learned important things from you about the experiment in general especially in the beginning of my work.

Nicht zu vergessen ist auch Florian Dufter, mein Bachelorandenkollege. Danke für deine Hilfe bei der LabView Software für das Keithley.

Ein weiterer Dank geht an Ralf Lang und den Rest der Werkstatt dafür, dass ihr immer die passenden Teile für mich gefertigt habt, auch wenn es mal schnell gehen musste.

Außerdem bedanke ich mich bei Dr. Michael Böhmer für die wichtigen und zahlreichen Ratschläge beim Design der COBRA GEMs.

Last but not least I want to thank the whole workgroup for adding me to the group really fast. This helped me feel comfortable at the new environment. Also you guys made the lunch breaks a lot of fun pretty often so thanks for that. It was a fun experience to be a part of you.